JOURNAL OF GEOPHYSICAL RESEARCH, VOL. 94, NO. C6, PAGES 8111–8124, JUNE 15, 1989

Shallow Water Application of the Third-Generation WAM Wave Model

LUIGI CAVALERI, LUCIANA BERTOTTI, AND PIERO LIONELLO

Istituto per lo Studio della Dinamica delle Grandi Masse, Consiglio Nazionale delle Ricerche, Venice, Italy

We present the results of detailed tests of the third-generation WAM wave model. The tests are carried out under well-known conditions, and they are chosen so as to check different aspects of the model. The test area is the Adriatic Sea, east of Italy, which is very shallow in its northern part. As expected from the basic physical approach of WAM to the problem, the results show the model's capability of responding equally well to different meteorological situations. Some discrepancies present at short nondimensional fetch and in shallow water are addressed with different formulations for breaking and bottom friction.

1. THIRD-GENERATION WAVE MODELS

The basic aim of the third-generation wave models is to approach the problem of the evaluation of the wave conditions from the physical point of view, avoiding many of the short cuts that are present in the models of the first and second generation. In the late seventies an increasing number of wave models were available. While their common target was the capability of correctly estimating the wave conditions in a given situation, many different approaches to the problem were proposed dependent on the specific situation in which each model was expected to work. Almost all the models had serious limitations in the mathematical representation of the physics of wind waves. This in turn led to bad performance when the models were required to operate out of the range for which they had been developed. All this was clearly shown by the Sea Wave Modeling Project (SWAMP) [*SWAMP Group*, 1985], an intercomparison test where all participating models were required to provide the results in a standard way to allow their effective comparison. The intercomparison test was composed of seven different cases of increasing complexity, starting with the simplest case of a uniform offshore wind and ending with a hurricane wind field. The geometry of the basins, wind fields, and location of the output points were all specified, so that input and output were identical for each model. The different results obtained were due to the differences between the models themselves.

The main conclusion of SWAMP was that if a major improvement in the performance of models was to be made, it would require accurate representation of all the physical terms relevant to wind wave growth and interaction processes. At the same time it was clear that such an approach was beyond the capability of any single group. A common approach was therefore necessary and the WAM (Wave Model) Group was formed, with the key characteristic of sharing ideas, programs, and results.

Other reasons also made a joint study necessary. Following the existence of global atmospheric models with up to 5 days of reliable forecasting capability (see, for example, *European Centre for Medium Range Weather Forecasts (ECMWF)* [1986]), it is only natural to use these models to drive a global wave model. As in this case we are going to deal with all the possible meteorological situations, the maximum reliability is connected to a physical approach to the problem. In addition, the ERS-1 satellite is expected to be launched in 1989, providing a large amount of wind and wave data over the oceans. Atmospheric and wave models must both be developed to allow data assimilation in real time on a global scale. Finally, as a given condition for the above realizations, there lie the latest achievements of the computer capabilities, in terms of both speed and storage.

Part of the above targets have already been achieved. A global version of the WAM wave model is now running daily at the ECMWF in Reading, England [*Janssen and Komen*, 1987]; extensive assimilation experiments have been carried out by *Janssen et al.* [1987].

A subgroup of WAM was formed to study the Mediterranean Sea and, especially, the Adriatic. An almost enclosed basin like the Adriatic has an important advantage for verification purposes compared with larger oceans: the meteorological conditions are well defined, and thus differences between model results and measurements are usually due to limitations of the physics in the WAM model. In particular, the large shallow areas of the Adriatic can provide a good test of dissipation processes which occur in limited water depths.

The WAM model has been extensively applied and tested in quite different situations. The *WAMDI Group* [1988] describes the results obtained both for Atlantic storms and for hurricanes in the Gulf of Mexico. *Zambresky* [1989] reports good results from the WAM global model as compared with the experimental data from more than 20 locations around the world (rms H_s error over 7 months is typically between 0.5 and 1.0 m). In these terms our main aim was not a simple confirmation of the model performance in a small basin, but rather a keen test of some of its aspects under well-defined conditions.

In this paper we describe the implementation of WAM in the Adriatic Sea and then discuss the obtained results and an alternative approach to part of the phenomenology. The paper is organized as follows. In section 2 we briefly outline the WAM model. Section 3 offers a description of the Adriatic Sea, its geometry, and its bordering orography. The different meteorological situations are discussed, and reasons are given for the choice of the storms. The available measured data are indicated. The actual implementation of WAM is shown, including a discussion on the accuracy of the grid representation. Section 4 includes the three hindcast experiments, corresponding to three different meteorological situations. The discussion of the results is in section 5,

Paper number 89JC00329.
0148-0227/89/89JC-00329$05.00

followed by the implementation of different approaches to wave breaking at short nondimensional fetch and to dissipation by bottom friction. This provides the results presented in section 6 followed by the final outlook in section 7.

2. The WAM Model

This section provides a compact description of the model. A much more extensive report is given by the *WAMDI Group* [1988].

It is assumed that wave conditions at a given time t and location ϕ and λ, where ϕ is latitude and λ is longitude, are represented by the two-dimensional spectrum $F(f, \theta, \phi, \lambda, t)$, f and θ being the frequency and direction that characterize the single wave component. The evolution of $F(\ )$ on the spherical Earth is governed by the transport equation

$$\frac{\partial F}{\partial t} + (\cos\phi)^{-1}\frac{\partial}{\partial \phi}(\dot{\phi}\cos\phi F) + \frac{\partial}{\partial \lambda}(\dot{\lambda} F) + \frac{\partial}{\partial \theta}(\dot{\theta} F) = S \quad (1)$$

where S represents the local source function and the dots represent derivatives with respect to time.

Specifically,

$$\dot{\phi} = vR^{-1}\cos\theta \quad (2)$$

$$\dot{\lambda} = v\sin\theta(R\cos\phi)^{-1} \quad (3)$$

$$\dot{\theta} = v\sin\theta\tan\phi R^{-1} \quad (4)$$

Here v is the group velocity and R is the radius of the Earth.

Equation (1) is a generalization to spherical geometry of the standard Cartesian geometry transport equation

$$\frac{\partial F}{\partial t} + \bar{v}\cdot\bar{\nabla}F = S \quad (5)$$

The left-hand side of the energy balance equation represents the propagation of wind waves, i.e., advection, and its solution is purely a mathematical problem. The physics of waves, the dynamics of the problem, is on the right-hand side term S that is divided into three parts,

$$S = S_{\rm in} + S_{\rm nl} + (S_{\rm br} + S_{\rm bf})_{\rm dis} \quad (6)$$

$S_{\rm in}$ represents the input of energy from the wind based on the Miles process,

$$S_{\rm in} = \beta F$$

where the expression for β is adopted from *Snyder et al.* [1981]. With respect to the original expression, the model uses a slightly modified version of β based, instead of on the 5-m height wind, on the friction velocity U_*. It is given by *Komen et al.* [1984] as

$$\beta = \max\left\{0.,\ 0.25\,\frac{\rho_a}{\rho_w}\left(28\,\frac{U_*}{c}\cos\theta_w - 1\right)\right\}\sigma \quad (7)$$

where $\sigma = 2\pi f$, ρ_a and ρ_w are air and water density, c is wave phase velocity, and θ_w is the angle between wind and wave direction.

$S_{\rm nl}$ represents the nonlinear, conservative, energy exchanges between all the possible quadruplets of wave components that satisfy given resonance conditions. Its evaluation requires enormous computer power and has been brought within the actual operational capabilities by the discrete interaction operator parametrization proposed by *Hasselmann et al.* [1985].

The accuracy of the procedure has been proved by direct comparison against the full calculation results done for different spectral shapes. In shallow water the nonlinear exchanges are corrected by a scaling factor evaluated according to *Herterich and Hasselmann* [1980]. The approximation is within acceptably small limits in the range $kd > 0.8$ (k is wave number, and d is depth). In the Adriatic Sea, where the peak period of storm spectra is around 10 s, this allows use of the model down to 16-m depth.

$S_{\rm dis}$ represents dissipation processes which can be conveniently split into "whitecapping" and bottom interaction processes. Whitecapping or breaking is the only relevant dissipation term in deep water. For its evaluation the model uses a modified version of the expression proposed by *Komen et al.* [1984], given as

$$S_{\rm br} = -2.33\times 10^{-5}\,\tilde{\omega}\left(\frac{\omega}{\tilde{\omega}}\right)^2\left(\frac{\tilde{\alpha}}{\tilde{\alpha}_{PM}}\right)^2 F \quad (8)$$

The tilde represents a slight approximation to the exact values, as for stability reasons, mean circular frequency $\tilde{\omega}$ is obtained as the inverse of the mean period. Specifically,

$$\tilde{\alpha} = E\tilde{\omega}^4 g^2 \quad (9)$$

$$\tilde{\alpha}_{PM} = 3.02\times 10^{-3} \quad (10)$$

E is the overall energy, and g is the acceleration of gravity.

The only bottom dissipation process permanently considered in the model is bottom friction. Other terms like percolation or viscoelasticity of the bottom material, relevant in certain specific areas, can be easily introduced if necessary. The bottom friction is expressed by

$$S_{\rm bf} = -\frac{\Gamma}{g^2}\frac{\sigma^2}{\sinh^2 kd}F \quad (11)$$

a parameterized expression deduced from the JONSWAP study [*Hasselmann et al.*, 1973] (hereinafter referred to as J) with the constant Γ = 0.038 $m^2\ s^{-3}$.

In the actual version the model considers 25 frequencies in geometric progression (f_1=0.0418 Hz, $f_{n+1}=1.1f_n$), and 12 directional bands with 30° resolution.

3. The Adriatic Sea

3.1. *Geography*

The Adriatic Sea (Figure 1*a*) lies east of Italy, enclosed between the Italian peninsula on one side and Yugoslavia and Albania on the other. It is an almost closed basin, the only connection with the Mediterranean Sea being the Otranto Strait to the south. The influence of this on the wave regime is only in the nearby region. As we discuss results in its northern section we consider the Adriatic as completely closed.

The geometrical shape is approximately rectangular, the main axis from northwest to southeast spanning about 750 km with 200 km across. The bottom slope is 1/1000 starting from 0 at the upper end until the edge of the continental platform (200-m depth) after which, with the exception of a narrow section close to the Italian coast, deepwater conditions hold. The currents are quite limited, with virtually no effect on waves. Possible exceptions are the Otranto Strait and the outflow of the river Po under particular outflow

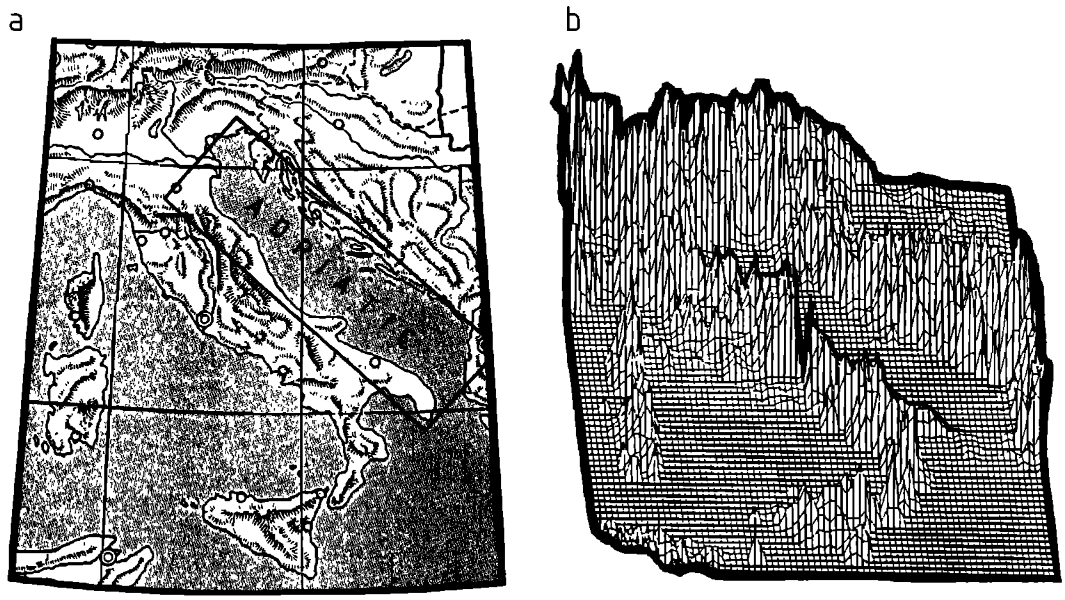

Fig. 1. (*a*) Map of Italy and border of grid in Figure 2. Note the orography bordering the Adriatic Sea. (*b*) Three-dimensional view of the area.

conditions. We have not considered their effects. Tidal currents are very small, of the order of 10 cm s^{-1} [*Franco et al.*, 1982].

The bordering orography is rather complicated (Figure 1*b*). The Alps close the system to the north, leaving only a connection to the Po valley. On the two main sides, the basin is practically enclosed between the Apennines (Italy) and the Dinaric Alps (Yugoslavia).

3.2. *Phenomenology*

Two main wind regimes are present (Figure 1). Bora, a cold northeasterly wind affecting the whole northern section of the basin, is associated with a high-pressure system over central Europe with sometimes a low-pressure center over southern Italy. This leads to a strong cold jet of dry air, extremely active, that causes highly generative, short-fetch wave conditions. The second regime is a southerly warm wind, scirocco, affecting the whole Adriatic Sea. Owing to the channeling effect of the Apennines and the Dinaric Alps, the surface wind blows along the main axis of the basin. Depending on the meteorological conditions, two possibilities exist at the northern end. If, as is typical of winter, a cold humid air layer lies on the Po valley, the warm scirocco passes above it. The surface evidence is that of a relatively active wind up to the Po mouth followed by flat calm, leading to pure swell at the northern coast. Alternatively, the scirocco reaches the northern end and then turns abruptly toward the west owing to the blocking effect of the Alps. In this case we find, in the north, cross-sea conditions with swell advancing at 90° with respect to the local wind.

3.3. *Wind Fields*

The evaluation of surface wind in the Adriatic Sea is not an easy task. On one side, the global three-dimensional model cannot resolve the complicated features and the strong spatial gradients present in the basin; there is experimental evidence of values up to 10^{-3} s^{-1} and 10^{-3} deg m^{-1} in stormy conditions. These values have been obtained by direct comparison of data recorded at the local meteorological station and at our oceanographic platform offshore (see below). On the other, the information is lacking for a possible three-dimensional model at local scale. In connection with other projects of our institute, this led us to develop a specific wind model for the Adriatic basin, based on the pressure values recorded at the various meteorological stations along the coast. No use can be made of locally recorded wind because of the dominant influence of local orography on it. The channeling effect of the mountain ridges is taken into account by an objective analysis of the pressure field, eventually correcting the field for the predetermined effect of the ridges. Wind is provided at synoptic times at the knots of a 40-km step size grid with axes fitted to those of the basin. A detailed description of the procedure and its accuracy is given by L. Cavaleri (Wind modeling in the Adriatic Sea, submitted to *Il Nuovo Cimento*, 1988).

3.4. *Measured Data*

Two main experimental stations are available in the Adriatic Sea. One is the oceanographic platform run by our institute, the Consiglio Nazionale delle Ricerche [*Cavaleri et al.*, 1981]. It is located 15 km off the coast of Venice at 16-m depth. It is equipped with meteorological and oceanographic instruments including anemometers and one directional wave-measuring system. The second is a Waverider buoy run by the Ente Nazionale Energia Elettrica (ENEL) placed in 25-m depth in front of the Po delta [*ENEL*, 1983]. The buoy was in operation up to 1983, when it was retrieved because of repeated problems with local fishing boats. Both systems provide wave spectra at 3-hour intervals at synoptic times. Their position is shown in Figure 2.

We have hindcasted eight storms using the WAM model. Of these, a three-storm subset has been chosen for discussion. They are characterized by very reliable wind fields, as confirmed by direct comparison with experimental data, and they represent the three basic meteorological situations described above. For these storms, only the ENEL wave data are available.

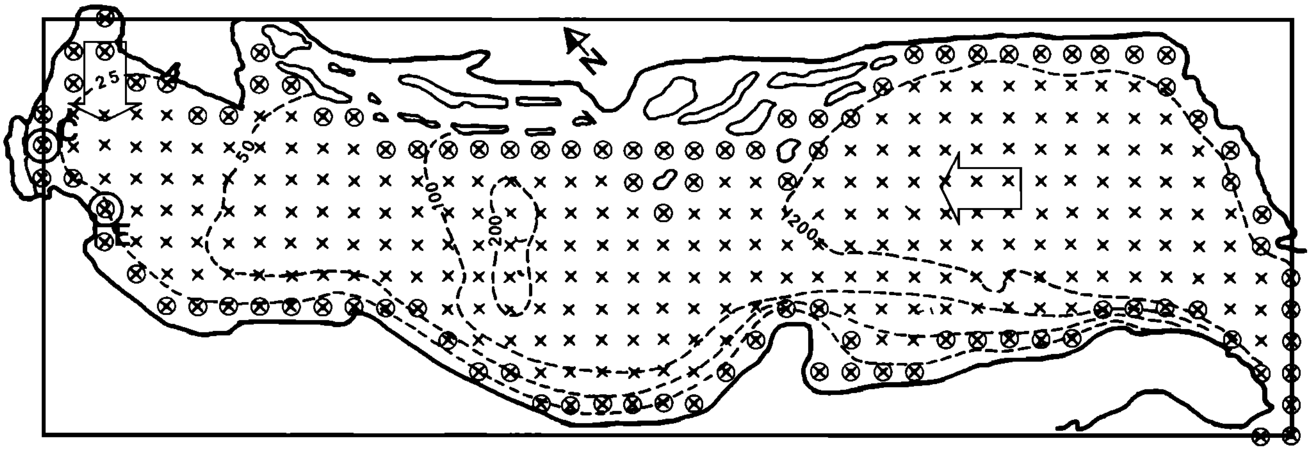

Fig. 2. Grid representation of the Adriatic Sea (see Figure 1*a*). The grid step is 20 km. The two large arrows show the main wind directions, bora from the northeast and scirocco from the southeast. C (oceanographic platform) and E (ENEL Waverider) mark the two recording stations.

3.5. *WAM Implementation*

The WAM model can be solved either on a geographic or a rectangular grid, using equation (1) or (5), respectively. As the Adriatic Sea is practically aligned at 45° with respect to the latitudinal and longitudinal directions, the former choice would lead to a very poor representation of the coast, with also numerical consequences for the advection term. On the other hand, there is no particular reason for such a choice, as we are not making use of any input from a global model based on geographical coordinates. Rather, as was mentioned in the preceding section, the wind grid we use is aligned along the basin axis, and it is natural to superimpose the wave grid on the wind one, with the further advantage of a very good representation of the coastal shape. We have therefore made use of (5).

There is an error associated with this choice due to the modification of the great circle paths followed by the wave trains. Together with the deformation associated with the Mercator projection of the map used for the grid, the maximum error is estimated to be less than 0.2%.

The WAM grid is shown in Figure 2. Its maximum dimensions are 43 × 16 points, with a 20-km grid size. In each direction, one point out of two is coincident with a wind grid knot. As the wind components must be specified at each wave grid point, they are linearly interpolated from the input wind field. A 15-min time step has been used for the integration of the advection and source terms.

The initial conditions are taken as a uniform J spectrum with significant wave height H_s = 0.25 m and mean period T_m = 3 s directed to north. The spin-up time of the model is approximately 12 hours.

4. Hindcast of Three Storms

4.1. *Case A: Bora With Very Active Generation Conditions*

On March 29–30, 1977, a very cold northeasterly wind blew over the northern Adriatic Sea. Wind speeds up to 20 m s^{-1} were recorded at the oceanographic platform. Air-sea conditions were highly unstable, with air colder than water by 10°C. In the area the waves were under very active, purely generative, fetch-limited conditions. The fetch in the wind direction was 120 km, decreasing on both sides because of coastal shape.

The wind field at 1500 UT on March 30 is shown in Figure 3*a*. Figure 4 provides a comparison between experimental and wind model data at the oceanographic platform. When weighted on the speed values, on the average the model underestimates the wind speed by 4% and it has 8° error in direction.

The wave field for the same time as in Figure 3*a* is shown in Figure 3*b*. Basically, the wave field follows the wind pattern. In the northern section the wave conditions are purely generative, with no influence from the south. This is confirmed by the two-dimensional spectra from the model.

Time history of significant wave height H_s and mean period T_m is given in Figure 5 (the thin dashed line in this figure and in Figures 7 and 10 refers to a modified version of the model discussed later.) Apart from the spin-up time, the model follows smoothly the storm, but it exhibits a tendency to overestimate the overall energy and the mean period. Owing to the recording technique (5-min record on graph paper), spectra were not available.

4.2. *Case B: Scirocco With Swell in the Northern Adriatic Sea*

On October 26–27, 1981, a scirocco wind blew over all the Adriatic Sea. Air-sea stability conditions were almost neutral. On the first day the wind affected also the northern part (20 m s^{-1} wind speed were recorded at the platform) leading to a relatively mild long fetch generation. Subsequently (Figure 6*a*) the wind was practically limited to the central and southern sections, leaving the north under a pure swell condition. The fit of the wind model at the platform is within 3% and 5° of the experimental data.

The wave field simultaneous to Figure 6*a* is in Figure 6*b*. It is virtually uniform in direction along the axis of the basin, growing in amplitude in the southern section (generation) and then placidly propagating to the northwest (swell).

The time history of H_s and T_m is shown in Figure 7. The fit between experimental and model results is very good for H_s, but the model overestimates T_m during the second day of the storm. The one-dimensional spectra for a late stage of the storm are shown in Figure 8. (All the spectra have 24 degrees of freedom; the associated 95% confidence interval is 0.6–1.9 [*Jenkins and Watts*, 1968, p. 82]).

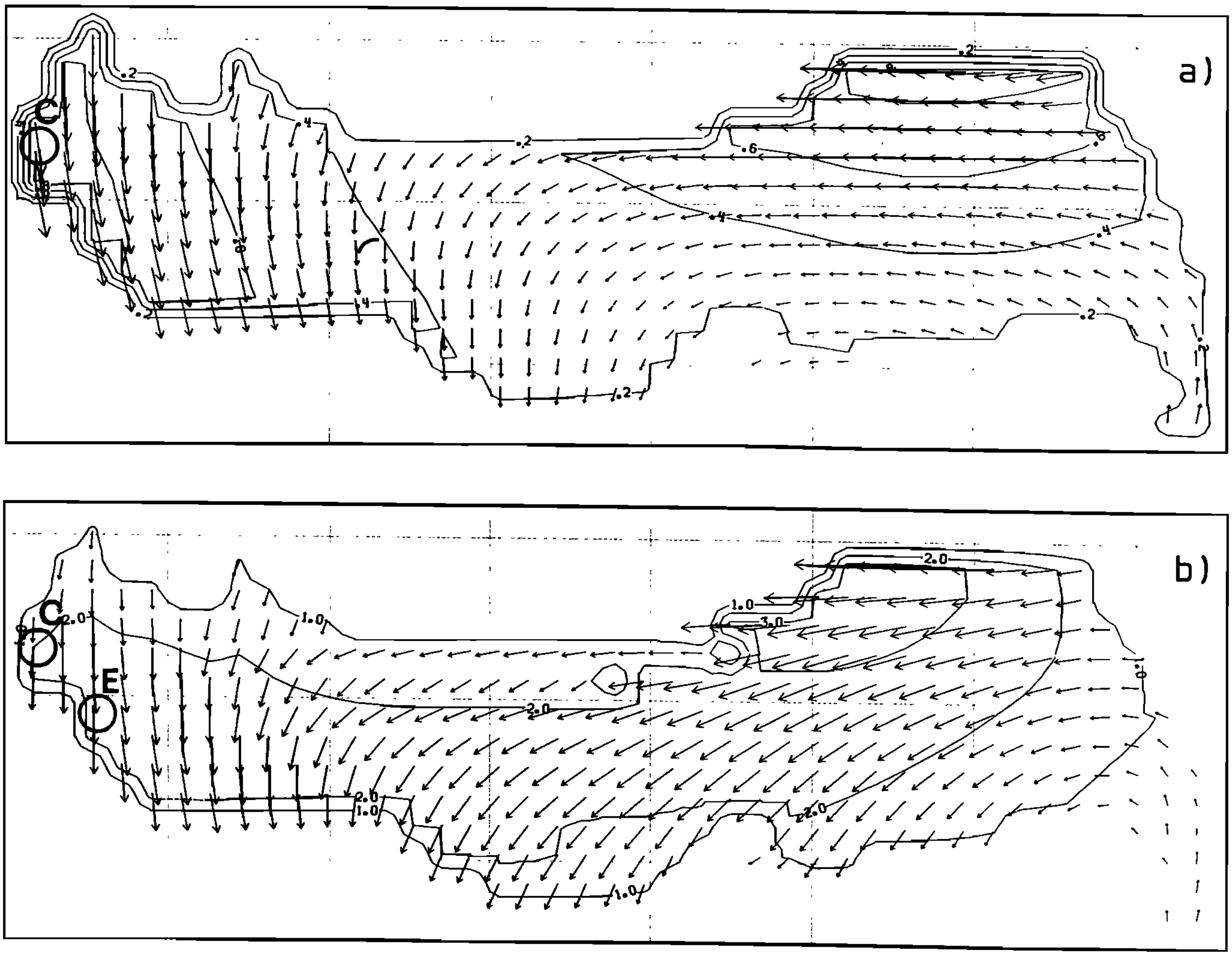

Fig. 3. (*a*) Wind field for 1500 UT on March 30, 1977. Arrows represent friction velocity. (*b*) Significant wave height for the same time as in Figure 3*a*. Isolines are in meters. C and E mark the two recording stations. The grid step is 20 km.

4.3. *Case C: Scirocco With Cross-Sea Conditions in the Northern Section*

From November 29 to December 2, 1982, a severe storm affected the whole Adriatic Sea. An intermittent scirocco wind blew in the central and southern sections, while a steadily intense northeast wind affected the northern part for the full 4 days (Figure 9*a*). The air-sea stability conditions were almost neutral in the south and highly unstable in the north. At the platform the wind model underestimates the wind speed by 5%, with zero degrees average error in direction. There is a strong flow of energy from the south (Figure 9*b*) that in the northern section interacts with northeasterly wind and the locally generated wave field. The time history of H_s and T_m is shown in Figure 10. During the first 2 days there is a good fit between model and experimental data for both H_s and T_m. Starting on December 1 the fit breaks down, and the model shows an increasing tendency to overestimate both parameters. The reasons for discrepancy are found upon examining the spectra. Figure 11 shows the one-dimensional spectra at 3000 UT on December 2. It is obvious that the model largely overestimates the low-frequency energy.

The different sea conditions existing at different times are clarified by the model two-dimensional spectra (Figure 12). At 3000 UT on December 1 the local wave conditions are purely generative. Twenty-four hours later, apart from a slight turn of the wind, the dominant feature is the heavy swell almost at cross angle to the wind. It is the source of most of the energy that causes the model overestimate on December 2.

5. DISCUSSION

In the following, reference will be made to the three cases (A, B, and C) described in the preceding section. Before proceeding further we stress again the accuracy of the wind fields. Cases A, B, and C have been selected out of a much larger set of 31 storms used to provide estimates of wave conditions in the northern Adriatic Sea. Out of this set, eight storms have been chosen as suitable for the verification of the WAM model. For each one of the eight storms, the wind fields have been carefully verified both by direct inspection of the maps and by comparison of the wind fields with all the available experimental data. This led to the final choice of the three storms in section 4. While explicit reference will be made to their results, we point out the self-consistency of the conclusions from the full subset of the eight storms.

We discuss first wave generation, then the energy loss by bottom friction.

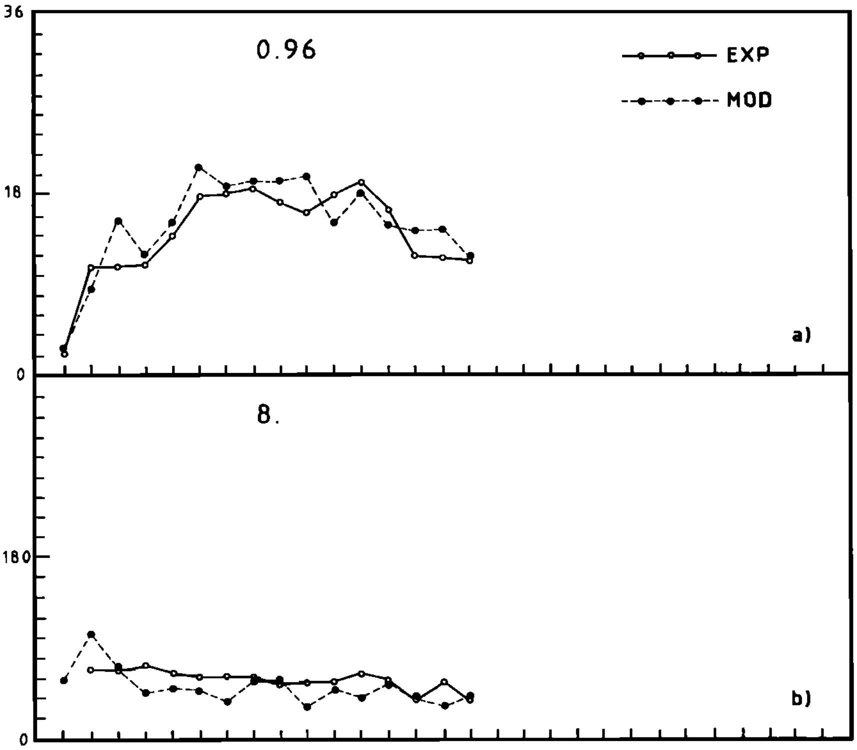

Fig. 4. Comparison between model (MOD) and experimental (EXP) wind data at the CNR oceanographic platform (position C in Figure 3a). (a) Modulus, in meters per second, The average ratio EXP/MOD is 0.96. (b) Direction, in degrees. The rms error is 8.

5.1. *Wave Generation*

Case A offers an example of pure generation conditions at the recording site. The overestimate of the model cannot be explained by a lack of accuracy of the instrumental position, as this would imply a shift of two or three grid steps. As a further test we have repeated case 2 of the *SWAMP Group* [1985], a uniform wind blowing orthogonally offshore a straight coast. The results are consistent with case A, i.e., compared with the J growth curve, the model overestimates energy at short nondimensional fetch. On the other hand, the *WAMDI Group* [1988] shows a remarkable agreement between the J and WAM growth curves. K. Hasselmann (personal communication, 1988) has pointed out that the discrepancy arises because of the insufficiently high resolution used for the grid. Having run case 2 with different resolutions, we have verified the sensitivity of the short-fetch results to the actual grid resolution. The conclusion is that, with an offshore wind, the first few grid points feel the effect of the border, and this effect is revealed as an overestimate of the overall energy. Afterward, the interacting sources take the model on the right trend.

This is a purely numerical effect. But, in our opinion, a more physical argument must also be considered. For this we consider the source function S in equations (1) and (5).

In section 2, S was split into three terms (equation (6)):

$$S = S_{in} + S_{nl} + (S_{br} + S_{bf})_{dis}$$

The term S_{nl} describing the nonlinear interactions is based on strong theoretical ground, and it has been verified by experiments (J). The wind input term S_{in} is based on the conclusions of *Snyder et al.* [1981] from the Bight of Abaco experiment. Both these references are very reliable and are widely accepted by the scientific community, and they will not be discussed further.

We are left with S_{dis}. Because of the depth distribution in the area, deepwater conditions hold for most of the generation. Also, at the ENEL position, a direct verification of the various source terms indicates S_{bf} to be at least 1 order of

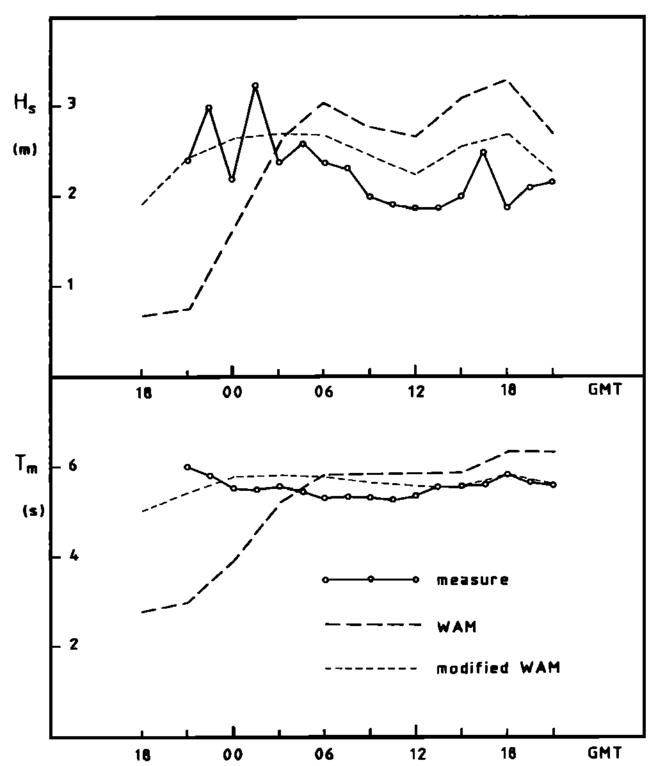

Fig. 5. Time history of significant wave height H_s and mean period T_m on March 29–30, 1977 (position E in Figure 3b).

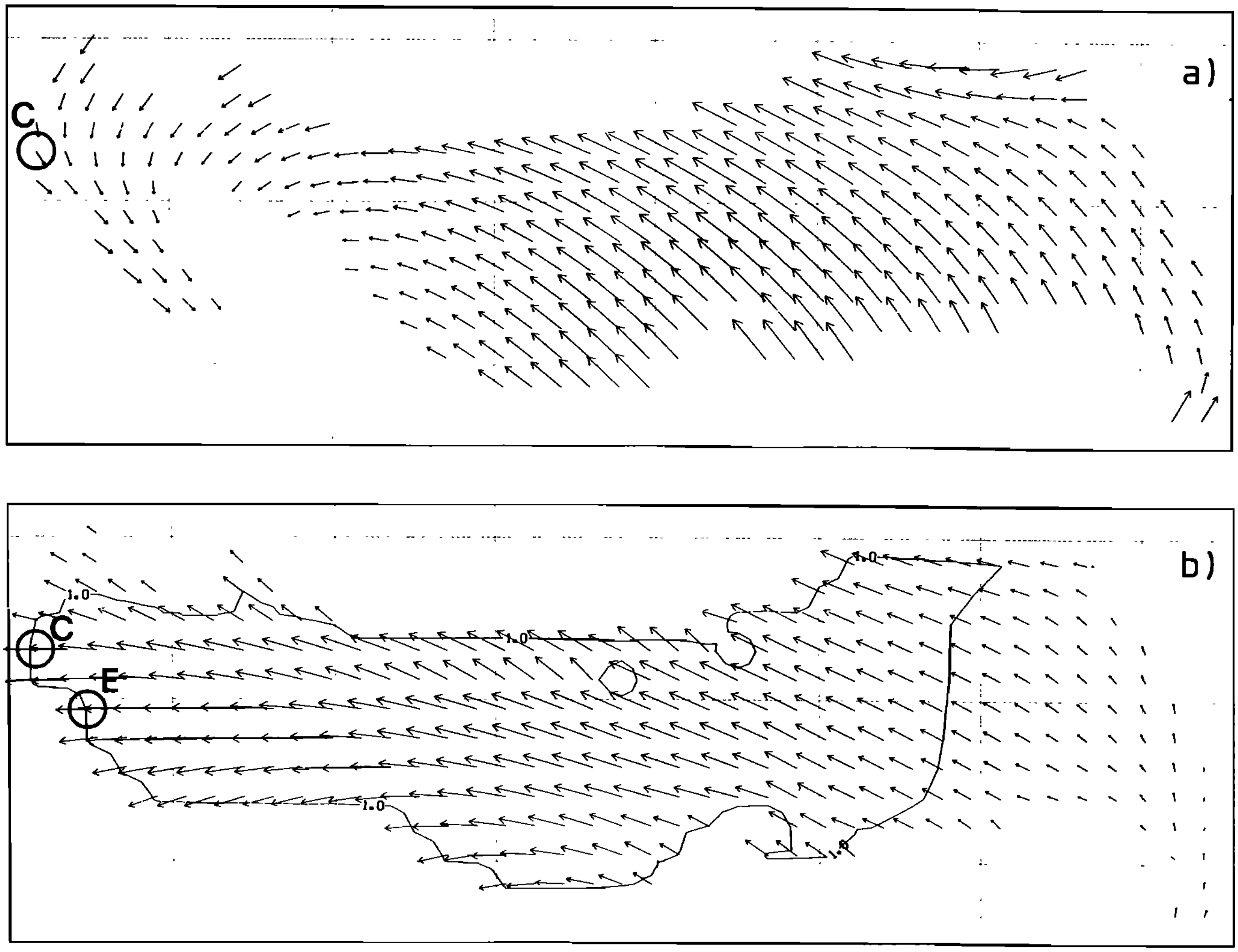

Fig. 6. (*a*) Wind field for 1800 UT on October 27, 1981. Arrows represent friction velocity. No isoline is traced as all the values are smaller than 0.2. (*b*) Significant wave height for the same time as in Figure 6*a*. Isolines are in meters. C and E mark the two recording stations. The grid step is 20 km.

magnitude smaller than S_{in} (S_{bf} will be discussed later, but the argument will remain.) Therefore we can confidently rule out S_{bf} as a possible reason for the discrepancy and concentrate our attention on S_{br}.

In the WAM model, coherently with *Hasselmann* [1974], the whitecapping is modelized with the general expression

$$S_{br} = c\bar{\omega}\left(\frac{\omega}{\bar{\omega}}\right)^2\left(\frac{\tilde{\alpha}}{\tilde{\alpha}_{PM}}\right)^m \tag{12}$$

where $\tilde{\alpha}$ and $\tilde{\alpha}_{PM}$ are given by (9) and (10). The c and m coefficients have been established by *Komen et al.* [1984] through the analysis of the dynamical equilibrium of the wave spectrum for conditions close to the fully developed stage. In this case, $\tilde{\alpha} \simeq \tilde{\alpha}_{PM}$, and the choice of m becomes unessential for the actual value of S_{br}. This is not the case for a young sea. By using the J growth curves of the dimensionless parameters, we estimate $\tilde{\alpha}/\tilde{\alpha}_{PM} = 1.5$ at the ENEL position, and we conclude S_{br} to be very sensitive to the value of m. This has been proved by G. van Vledder (personal communication, 1988), who has checked the duration-limited growth curve of the exact nonlinear model [*SWAMP Group*, 1985] for different m values in (12). After 10^4 s, a time interval that for wave growth can roughly be compared with our fetch conditions, H_s drops from 3.82 m for $m = 2$ to 3.10 for $m = 3$. This is coherent with the overestimate we reported for cases A and C.

In the actual formulation (see (8) and (12)) the loss by whitecapping depends only on the wave spectrum, not on the wind, and this is somehow unrealistic. Certainly an implicit dependence is hidden in (8) and (12), because $\tilde{\alpha}$, the integral wave steepness given by (9), depends on the previous wind fields. But the breaking is a local phenomenon, and direct sea experience confirms that for given wave conditions, a sudden increase in the wind speed produces an abrupt strong increase in the number of breakers and of the associated energy loss. There is ample experimental evidence in this sense (see, for example, *Toba and Koga* [1986]). In the early stages of development, breaking is highly frequent; this can weaken the basic hypothesis [*Hasselmann*, 1974] that the whitecapping is strong locally but weak in the mean. Therefore it should not be surprising that the theory, and consequently expression (8), does not fit the experimental data for limited fetch or duration. At later stages, when the phase speed at the peak becomes comparable to the wind speed, the wind influence can be expected to decrease, and the whitecapping can be expected to become weak in the mean and therefore to be correctly described by (8). Confirmation in this sense is given by case

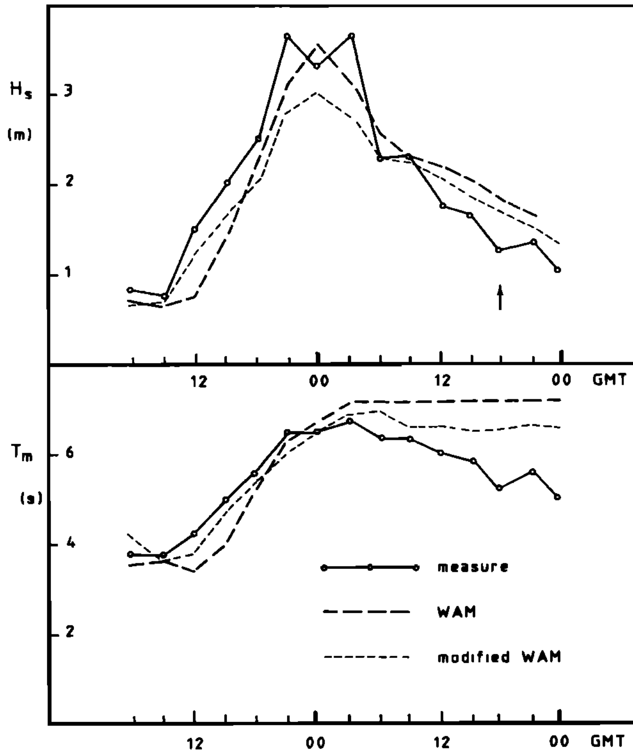

Fig. 7. Time history of significant wave height H_s and mean period T_m on October 26–27, 1981 (position E in Figure 6*b*). The vertical arrow indicates the time of the spectrum shown in Figure 8.

B, a long-fetch moderate generation with large nondimensional fetch, where (see Figure 7) the WAM model smoothly reproduces the experimental trend.

A full attack on the problem is outside the scope of this paper. We have, however, carried out some sensitivity tests by changing the m value in (12). Figure 13 compares the J and WAM growth curves, the latter obtained with $m = 2$ and $m = 3$, respectively. The grid resolution was 0.25°, about 28 km. As expected, the increased energy loss by breaking leads to comparably less energy at similar fetch. While the spectrum develops, $\tilde{\alpha}$ in (12) approaches $\tilde{\alpha}_{PM}$, and breaking becomes independent of m.

We have considered also the possibility of a variable m during growth. Following the above discussion, a suitable quantity for the parametrization of breaking is c_P/U, the ratio between the phase speed at the spectral peak and the wind speed. We have used the expression

$$m = 3 - 2c_P/U \qquad (13)$$

The resulting growth curve is shown in Figure 13. Alternative expressions for m can easily be thought of, for instance, dropping 2 in (13), or letting m shift from 3 at the early stages of development to 2 at fully developed conditions. The main point we want to stress is that at short nondimensional fetches a correct representation of breaking is likely to require proper consideration of the interaction between the wave spectrum and the local wind.

5.2. *Bottom Friction*

In the preceding section, case B has offered an example of swell from southeast with a correct evaluation of the energy present in the northern part. On the contrary, in case C, where swell interacts heavily with the local wind waves, our H_s estimate is in excess, mainly because the low-frequency energy is overestimated.

The interaction of wind waves with the bottom is basically through one or more of the following phenomena: backscattering, percolation, elasticity of the bottom material, and bottom friction. We consider them in sequence.

The scattering of surface waves by an irregular bottom has been analyzed by *Hasselmann* [1966] and *Long* [1973]. The phenomenon is energy conservative, its effect being a redistribution of energy among the wave components including those propagating in a direction opposite to that of the incoming waves. *Long* [1973] has used scattering to explain the experimental swell attenuation in J. The conditions were similar to those we are analyzing in the Adriatic Sea (depth between 10 and 30 m, $f_P \simeq 0.1$ Hz). Long showed that the experimental evidence could be justified by bottom irregularities with 60-cm rms amplitude and bottom wavelength between 50 and 500 m (range of surface wave length). For the same range the corresponding amplitude in the northern Adriatic is of the order of a few centimeters. As the scattering efficiency is proportional to the square of the amplitude, we can rule out this effect for practical consideration. In addition, we have analyzed some heavy swell cases directionally recorded at the CNR platform (Figure 2) by the variational technique of *Long and Hasselmann* [1979]. In no case have we found evidence of energy traveling against the incoming swell direction.

Percolation is the flow in the bottom material induced by the wave pressure field discussed earlier. Its importance, in terms of energy loss, with respect to other mechanisms has been analyzed by *Shemdin et al.* [1980]. They find the effect to be minor for a mean sand diameter of 0.38 mm, and to decrease rapidly with it. In the northern Adriatic, the mean sand diameter is 60 μm, and the effect is consequently negligible.

If the bottom material has some degree of elasticity, it reacts with vertical alternative movements to the wave

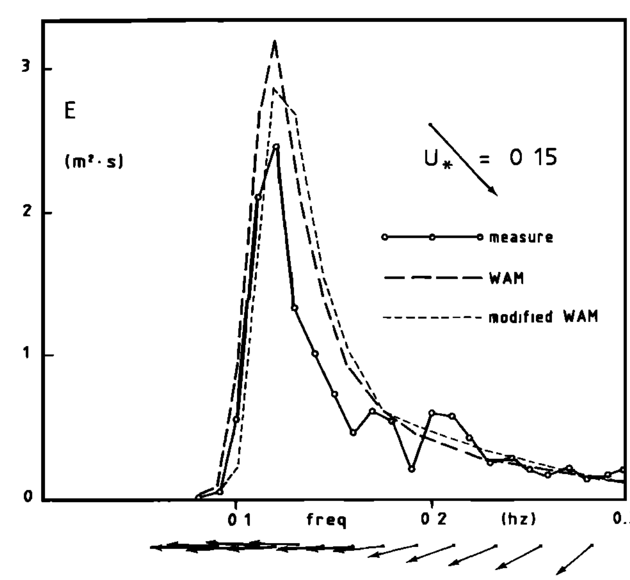

Fig. 8. One dimensional spectra at position E at the same time of Figure 6*b*. The large arrow shows the direction of local wind. The small arrows indicate the mean direction of each wave component out of the model. The reference for direction is Figure 6.

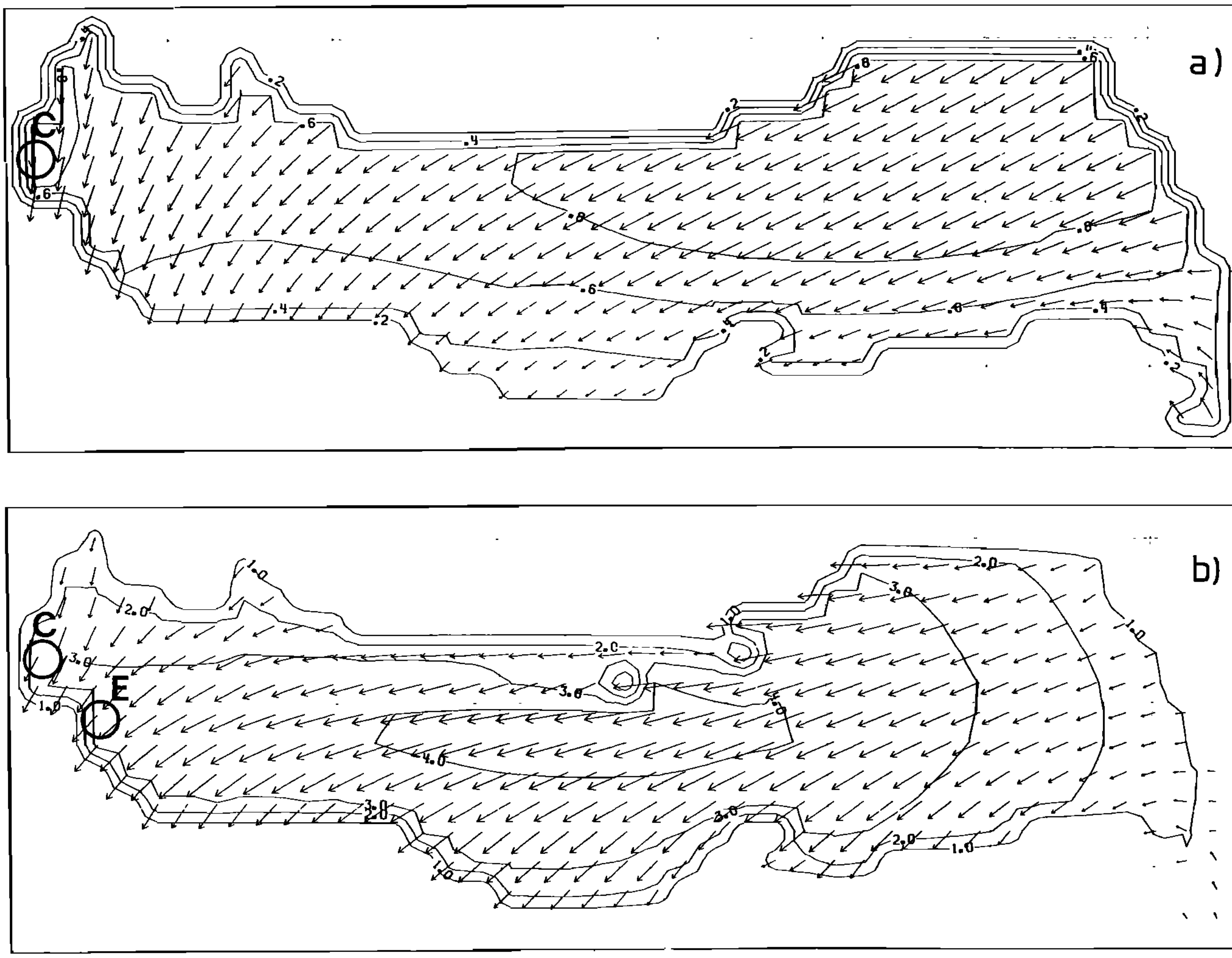

Fig. 9. (*a*) Wind field for 0000 UT on December 2, 1982. Arrows represent friction velocity. (*b*) Significant wave height for 0300 UT on the same day. Isolines are in meters. C and E mark the recording stations. The grid step is 20 km.

pressure fields. The eventual energy absorption depends on its viscous characteristics. Usually, this effect is irrelevant for sand, and *Rosenthal* [1978] has analyzed its influence for J swell cases. He found the effect to be more than 1 order of magnitude smaller than is needed to explain the attenuation. Accordingly, we do not consider it a possible explanation for swell attenuation in our case.

We are therefore left with the bottom friction that as was mentioned previously and as is coherent with the above considerations, is the only mechanism present in the WAM model. Physically, energy is lost because of the work done by the wave orbital velocity against the bottom turbulent shear stress. The fact that the shear stress

$$\tau = c_f \rho_w u_b^2 \tag{14}$$

depends, via the drag coefficient c_f and the water density ρ_w, on the square of the horizontal bottom velocity u_b implies both nonlinearity and coupling among different components. The theory has been developed by *Hasselmann and Collins* [1968] (hereinafter referred to as H-C) and an approximate treatment used by *Collins* [1972] for shallow water calculations. Assuming c_f constant throughout the wave cycle and, according to previous experimental results, equal to 0.015, his dissipation function reads

$$S_{bf}(f, \theta) = -\frac{c_f g k v}{2\pi\sigma^2 \cosh^2 kh} F(f, \theta)\langle u\rangle \tag{15}$$

with $\langle u\rangle$, the ensemble average of the modulus of the bottom orbital velocity, defined as

$$\langle u\rangle^2 = \sum_f E(f) \frac{g^2 k^2}{\sigma^2 \cosh^2 kh} \Delta f \tag{16}$$

The WAM formulation for bottom friction (equation (11)) is taken directly from J. There swell was not very intense, and the bottom velocity was dominated by tidal currents. In the first approximation this allowed us to neglect the effects of nonlinearity and any interaction among frequencies, producing the linear and decoupled expression (11): this assumption cannot be assumed to hold in general. It is certainly not true in the northern Adriatic, where orbital velocities dominate over the weak currents present in the area. In fact, we have taken the opposite assumption and neglected any influence of tidal and mean currents.

We have carried out a detailed analysis of the two approaches, linear and nonlinear, to the representation of bottom friction, and of their quantitative differences. While the full results are reported elsewhere (L. Cavaleri and P. Lionello, Linear and nonlinear approach to bottom friction

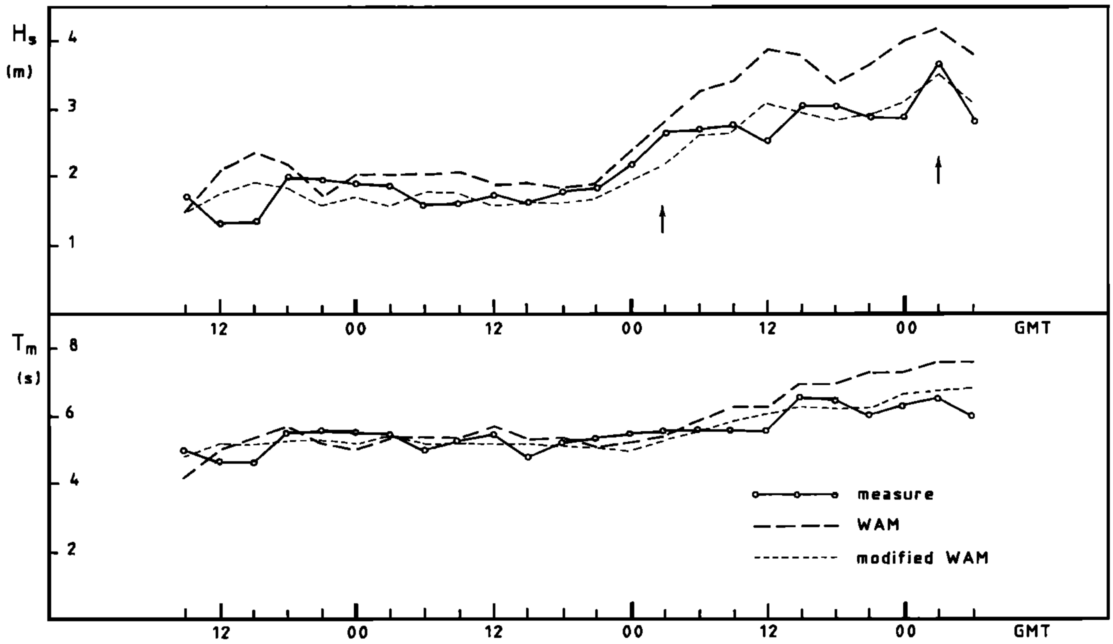

Fig. 10. Time history of significant wave height H_s and mean period T_m from November 29 through December 2, 1982 (position E in Figure 9*b*). The vertical arrows indicate times of the spectra shown in Figures 11 and 12.

in wave motion: Critical intercomparison, submitted to *Estuarine, Coastal, and Shelf Science*, 1989) we summarize here our main findings.

We define $S_{\text{H-C}}$ and S_J as the source terms from bottom friction according to H-C and J theory, respectively. By direct inspection of (11) and (15) we find that for a given wave component, the ratio $r = S_{\text{H-C}}/S_J$ depends only on $\langle u \rangle$. This implies that $r = 1$ only for a certain value of $\langle u \rangle$, above (below) which the linear approach underestimates (overestimates) the energy loss. This is what we expect from a nonlinear process such as (14).

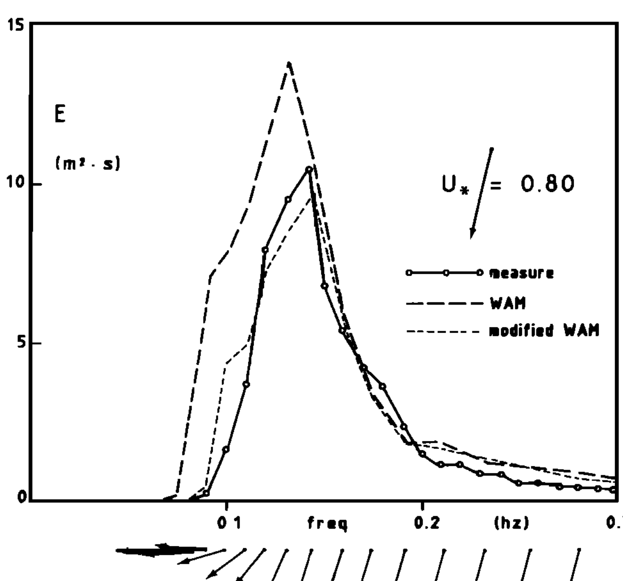

Fig. 11. One-dimensional spectra at position E at the time of Figure 9*b*. The large arrow shows the direction of local wind. The small arrows indicate the mean direction for each frequency. The reference for direction is Figure 9.

A more comprehensive feeling is obtained by comparing the overall energy loss in the spectrum. From the H-C theory this is given by

$$S_{\text{H-C}}(\mathbf{k}) = \frac{c_f g k^2 F(\mathbf{k})}{\sigma^2 \cosh^2 kh} \cdot \left[\langle u \rangle + \cos^2 (\phi - \theta) \left\langle \frac{u_x^2}{u} \right\rangle + \sin^2 (\phi - \theta) \left\langle \frac{u_y^2}{u} \right\rangle \right] \quad (17)$$

where (u_x, u_y) are orthogonal components of u with u_x directed along the main direction ϕ.

Given $F(k)$, the integral of (17) can be obtained only by numerical integration. An enlightening result is obtained on assuming a constant directional distribution throughout the spectrum. In this case the integral ratio r between the overall energy losses is given by

$$r = \frac{c_f g}{\Gamma} \int_0^{2\pi} \left[\langle u \rangle + \cos^2 \theta \left\langle \frac{u_x^2}{u} \right\rangle + \sin^2 \theta \left\langle \frac{u_y^2}{u} \right\rangle \right] D(\theta)\, d\theta \quad (18)$$

where, without any loss in generality, we have taken $\phi = 0$. $D(\theta)$ is the directional distribution satisfying the condition

$$\int_0^{2\pi} D(\theta)\, d\theta = 1$$

For a given $D(\theta)$ the quantities $\langle u_x^2/u \rangle$, $\langle u_y^2/u \rangle$ are linear in $\langle u \rangle$, say,

$$\left\langle \frac{u_x^2}{u} \right\rangle = a\langle u \rangle \qquad \left\langle \frac{u_y^2}{u} \right\rangle = b\langle u \rangle$$

with a and b suitable quantities less than 1. Hence (18) can be written

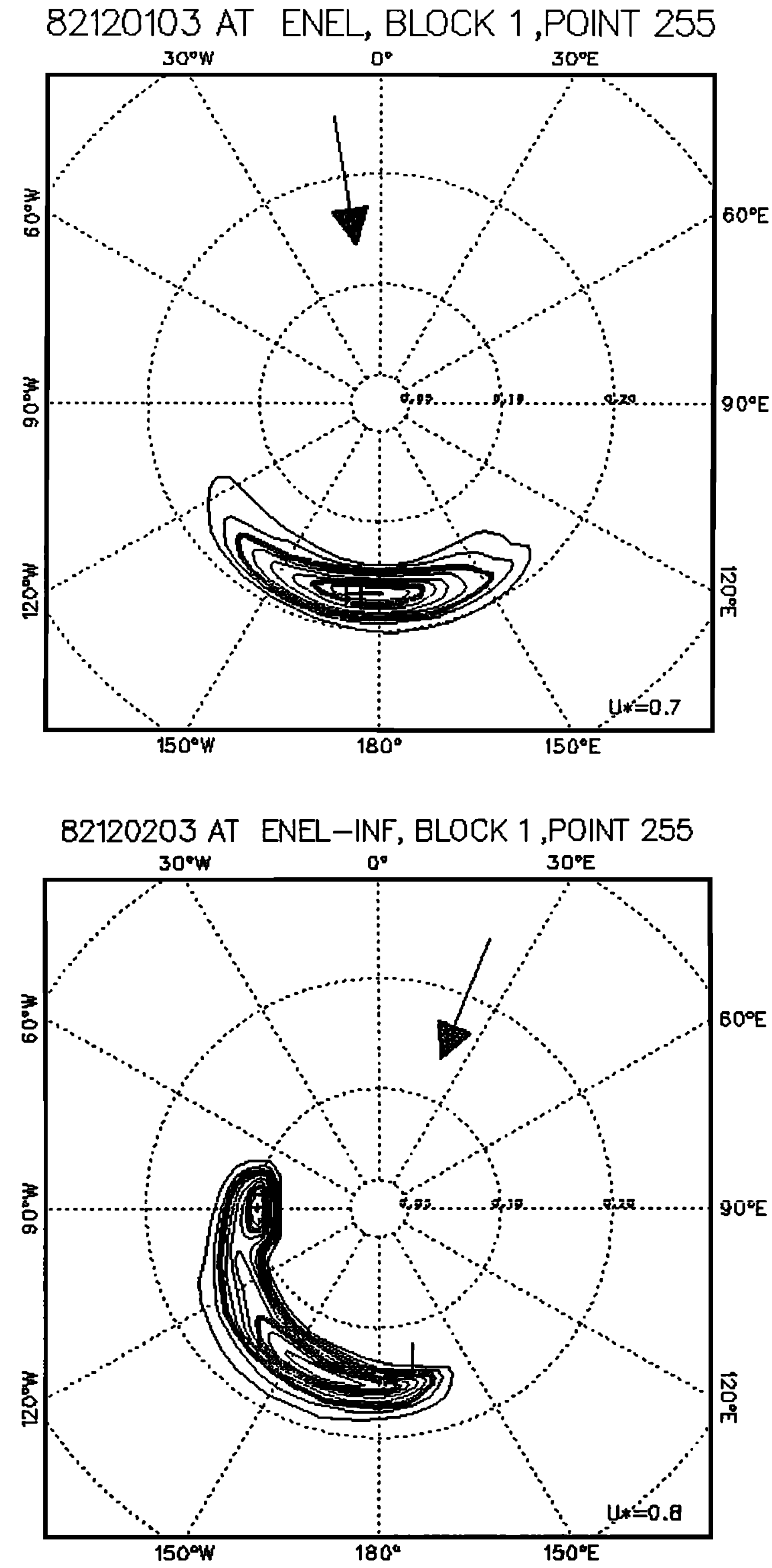

Fig. 12. Two-dimensional spectra at position E (see Figure 9*b*) at 0300 UT on December 1 and 2, 1982.

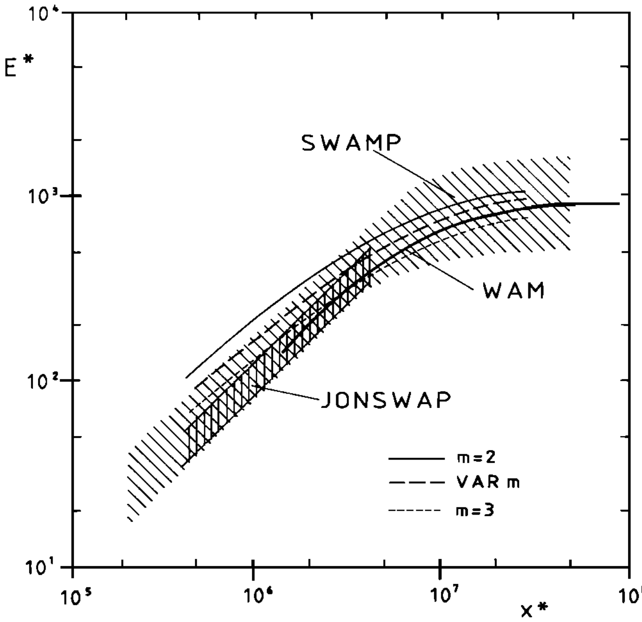

Fig. 13. Nondimensional fetch-limited growth curves for the total energy E^* [from *WAMDI Group*, 1988]. Superimposed (dashed lines) are tests with 0.25° grid step, $m = 2$ WAM model, $m = 3$ enhanced breaking, and variable m coefficient (var m).

$$r = \frac{c_f g}{\Gamma} \langle u \rangle \int_0^{2\pi} [1 + a \cos^2 \theta + b \sin^2 \theta] D(\theta)\, d\theta$$

$$= \frac{c_f g}{\Gamma} \langle u \rangle G(D(\theta))$$

with G a function of the directional distribution only. So, for a given $D(\ )$, r depends only on $\langle u \rangle$, independently of the energy distribution in the one-dimensional frequency spectrum. Table 1 provides, for different directional distributions, the $\langle u \rangle$ values for which $r = 1$. These values turn out to be similar to the ones measured during the JONSWAP experiments, which cannot be any surprise, because these are the values on which the linear expression (11) has been calibrated.

The above arguments are better summarized by observing the time energy decay of a JONSWAP spectrum, according to the H-C and J theories. The results, for different depth and initial peak frequency, are shown in Figure 14. At relatively low wave height the J approach is acceptable. At even smaller H_s its overestimate has no great consequences, at least for short times or distances, because the energy involved is small. The difference from the nonlinear approach becomes substantial for high wave heights. In this case, when also the energy involved in the process is large, the linear approach underestimates the energy attenuation by 50%.

TABLE 1. Values of $\langle u \rangle$ for Which $r = 1$

Directional Distribution	$\langle u \rangle$,* cm s^{-1}
$\cos^2$	16.17
$\cos^4$	15.37
$\cos^8$	14.57

*Ensemble average of bottom orbital velocity modulus. The value of $\langle u \rangle$ for which linear and nonlinear approaches to bottom friction produce identical results depends on the directional distribution.

A practical example is given by the Texel storm, discussed in detail by *Bouws and Komen* [1983]. The wave conditions were remarkable for intensity and constancy in time: $u = 25$ m s^{-1}, $H_s = 6.8$ m, $f_P = 0.09$ Hz, and $d = 35$ m. Bouws and Komen analyze the dynamic equilibrium of the spectrum using expression (11) for bottom friction, and they find it possible only by increasing Γ of a quantity between 50 and 75%. This is the corresponding increase in bottom friction dissipation we have found by using the nonlinear approach on the same figures.

The left side of Figure 14, with $H_s = 2.5$ m, corresponds to case A, and it is a clear indication that (as was already pointed out) bottom friction does not play a major role here. The right-hand side presents the typical scirocco conditions, and the two cases considered ($H_s = 2.5$ m, $H_s = 5$ m) tend to represent the conditions prevalent in cases B and C, respectively. Their results, the good fit for the low swell in B and the large overestimate for the heavy sea conditions in C, now have their logical explanation.

6. REPEATED HINDCAST OF THE THREE STORMS

Following the discussion in the previous section, we have repeated the hindcast of the three storms with the following modifications: for breaking, $m = 3$ in expression (12) and for bottom friction, H-C theory is substituted for J theory. The results are shown again in Figs. 5, 7, and 10 by the thin dashed lines. The new runs were started a few hours in advance, so there is no spin-up period in their plots. Excluding this from the comparison, the H_s rms error has changed from 1.05, 0.42, and 0.61 to 0.57, 0.42, and 0.25 meters for cases A, B, and C, respectively. The values of mean period T_m show even more drastic improvements (Table 2).

Our conclusions are as follows. Case A is the least satisfactory. This was expected, as the suggested modifica-

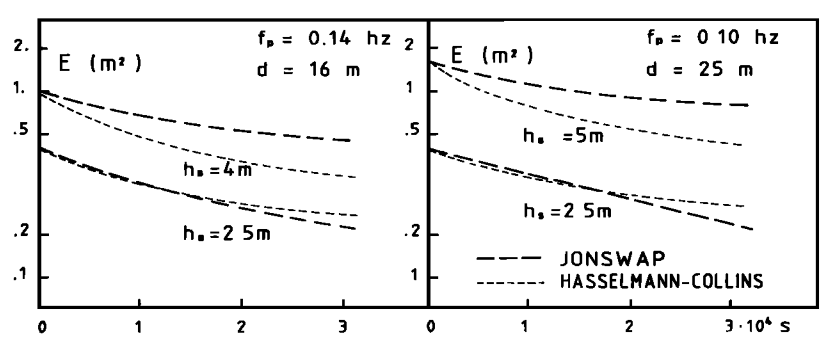

Fig. 14. Time decay, due to bottom friction, of the overall energy of a JONSWAP spectrum.

TABLE 2. Root-Mean-Square Error of H_s and T_m Estimates Obtained With WAM and Modified WAM Models

	H_s, m		T_m, s	
Case	WAM	Modified WAM	WAM	Modified WAM
A	1.05	0.27	0.60	0.27
B	0.42	0.42	1.13	0.72
C	0.61	0.25	0.63	0.25

tion for breaking has no theoretical background. Also, the mentioned effect of grid resolution, even if not the only one, is likely to be a reason for discrepancy. Case B has the least spectacular results. The reasons are (1) the long fetch with relatively mild generation, where the arguments used on discussing the breaking lose their effect, and (2) the low swell, suitable for the linear approach to bottom friction. We are quite satisfied with case C. It certainly provided the best results, and this followed the improvement in the description of bottom friction, something of which we feel we understand the physics.

7. OUTLOOK

One of the main characteristics of the third-generation WAM model is to avoid as many short cuts as possible in the description of the physics of wind waves. Even if because of insufficient knowledge or computer limitations we have only a crude description of a physical phenomenon in some cases, each process is described independently of the others. When a better description becomes available, this will allow its immediate implementation into the model. The modular structure of the model makes this a straightforward operation.

In testing the new description of a physical process, two different lines of attack are usually available. In one case a large extensive test is carried out, for instance, running a 1-month hindcast on a wide ocean. The results with and without the "improvement" are then compared, and a conclusion about it is finally reached. Alternatively, one can concentrate on a few specific cases, aiming at a very thorough analysis of each case, from which specific conclusions are possible for the single terms of the equation. The two approaches have clearly different aims. The former provides a general validation of the model in its various possible shapes, and the latter focuses the attention on the single terms, trying to reach conclusions about the correctness of their formulation. This can be done only under very simplified conditions, some sort of natural SWAMP cases, for which reliable input wind fields are available. This is what we have done in the "Adriatic laboratory," and in our opinion the results confirm our belief.

The implementation of the nonlinear bottom friction will not affect the general performance of the global model described by the *WAMDI Group* [1988]. Obviously, the improvement will appear only on the few large shallow areas of the globe. The Gulf of Mexico, the Argentine continental shelf, and the southern North Sea are notable areas in this sense. The consequences will be more general as high-resolution models are developed for specific areas, most of them on the continental shelf close to the coast, where strong economic interests are concentrated. Even if the major storms will be coming from the open sea, the ability to produce an accurate estimate of wave conditions also when the wind blows toward the open sea is of obvious concern. For this we see two possible solutions. The first is to envelop the lands with a high-resolution grid nested in the large one. This would provide a very accurate description of the coastal shapes and of the local bathymetry, and it would suit the accuracy of the results. We expect this solution to be used in the future, but we judge it problematic with the computer power currently available. The second solution we suggest is whenever the wind blows toward the sea, to impose a JONSWAP spectrum at each coastal point, evaluated according to local fetch, wind speed, and directon. If our considerations on breaking are correct, in most cases at one grid step off the coast the waves will be already within the range of validity of the *Hasselmann* [1974] theory. The grid resolution would not be a problem, as with a correct result at the first grid point, the influence of the border would be already forgotten.

Acknowledgments. Several members of the WAM community offered helpful discussion during the analysis of the results. In particular Peter Janssen, under ESA contract at ECMWF during our use of the local computer facilities, was a generous source of information on the model implementation. John Ewing made helpful suggestions on the final version of the paper. It is difficult to express appropriate gratitude to the personnel of ECMWF. They have done much more than we could hope to smooth our way. But we want in particular to thank Norbert Kreitz, who devoted so much of his time to us to almost credit the co-authorship of the paper.

REFERENCES

Bouws, E., and G. J. Komen, On the balance between growth and dissipation in an extreme depth-limited wind-sea in the southern North Sea, *J. Phys. Oceanogr.*, *13*, 1653–1658, 1983.

Cavaleri, L., S. Curiotto, G. Dallaporta, and A. Mazzoldi, Directional wave recording in the northern Adriatic Sea, *Nuovo Cimento*, *4C*(5), 519–534, 1981.

Collins, J. I., Prediction of shallow-water spectra, *J. Geophys. Res.*, *77*(15), 2693–2707, 1972.

Ente Nazionale Energia Elettrica (ENEL), Studio del moto ondoso lungo le coste italiane—Porto Tolle, 1982, *Rep. SI-632/83*, 99 pp., Dir. Stud. e Ricerche, Cent. di Ric. Idraul. e Strutturale, Venice, Italy, May 1983.

European Centre for Medium Range Weather Forecasts, *Rep. 35*, 39 pp., Reading, England, 1986.

Franco, P., L. Jeftic, P. Malanotte Rizzoli, A. Michelato, and M. Orlic, Descriptive model of the Northern Adriatic, *Oceanol. Acta*, *5*(3), 379–389, 1982.

Hasselmann, K., Feynman diagrams and interaction rules of wave-wave scattering processes, Rev. Geophys., *4*(1), 1–32, 1966.

Hasselmann, K., On the spectral dissipation of ocean waves due to white capping, Boundary Layer Meteorol., *6*, 107–127, 1974.

Hasselmann, K., and J. I. Collins, Spectral dissipation of finite-depth gravity waves due to turbulent bottom friction, *J. Mar. Res.*, *26*(1), 1–12, 1968.

Hasselmann, K., T. P. Barnett, E. Bouws, H. Carlson, D. E. Cartwright, K. Enke, J. A. Ewing, H. Gienapp, D. E. Hasselmann, P. Kruseman, A. Meersburg, P. Müller, D. J. Olbers, K. Richter, W. Sell, and H. Walden, Measurements of wind-wave growth and swell decay during the Joint North Sea Wave Project (JONSWAP), *Dtsch. Hydrogr. Z.*, 8(12), suppl. A, 95 pp., 1973.

Hasselmann, S., K. Hasselmann, J. H. Allender, and T. P. Barnett, Computations and parameterizations of the nonlinear energy transfer in a gravity-wave spectrum, II, Parameterizations of the nonlinear energy transfer for application in wave models, *J. Phys. Oceanogr.*, *15*, 1378–1391, 1985.

Herterich, K., and K. Hasselmann, A similarity relation for the nonlinear energy transfer in a finite-depth gravity-wave spectrum, *J. Fluid Mech.*, *97*(1), 215–224, 1980.

Janssen, P. A. E. M., and G. J. Komen (Eds.), *WAM Newsl. 2*, 4 pp., K. Ned. Meteorol. Inst., de Bilt, The Netherlands, 1987.

Janssen, P. A. E. M., P. Lionello, M. Reistad, and A. Hollingworth, A study of the feasibility of using sea and wind information from the ERS-1 satellite, 2, Use of scatterometer wind and altimeter data in wave modelling and assimilation, report, 42 pp., Eur. Space Agency, Paris, 1987.

Jenkins, G. M., and D. G. Watts, *Spectral Analysis and Its Application*, 256 pp., Holden-Day, San Francisco, Calif., 1968.

Komen, G. J., S. Hasselmann, and K. Hasselmann, On the existence of a fully developed windsea spectrum, *J. Phys. Oceanogr.*, *14*, 1271–1285, 1984.

Long, R. B., Scattering of surface waves by an irregular bottom, *J. Geophys. Res.*, *78*(33), 7861–7870, 1973.

Long, R. B., and K. Hasselmann, A variational technique for extracting directional spectra from multi-component wave data, *J. Phys. Oceanogr.*, *9*(2), 373–381, 1979.

Rosenthal, W., Energy exchange between surface waves and motion of sediment, *J. Geophys. Res.*, *83*(C4), 1980–1982, 1978.

Sea Wave Modeling Project (SWAMP) Group, *Ocean Wave Modeling*, pp. 37–47, Plenum, New York, 1985.

Shemdin, O. H., S. V. Hsiao, H. E. Carlson, K. Hasselmann, and K. Schulze, Mechanisms of wave transformation in finite-depth water, *J. Geophys. Res.*, *85*(C9), 5012–5018, 1980.

Snyder, R. L., F. W. Dobson, J. A. Elliott, and R. B. Long, Array measurements of atmospheric pressure fluctuations above surface gravity waves, *J. Fluid Mech.*, *102*, 1–59, 1981.

Toba, Y., and M. Koga, A parameter describing overall conditions of wave breaking, whitecapping, sea-spray production and wind stress, in *Oceanic Whitecaps and Their Role in Air-Sea Exchange Processes*, edited by E. D. Monahan and G. Mac Niocaill, 294 pp., D. Reidel, Norwell, Mass., 1986.

WAM Development and Implementation (WAMDI) Group, The WAM model—A third generation ocean wave prediction model, *J. Phys. Oceanogr.*, *18*(12), 1988.

Zambresky, L. F., A verification study of the global WAM model December 1987–November 1988, *Rep. 63*, Eur. Centre for Medium Range Weather Forecasts, Reading, England, 1989.

L. Bertotti, L. Cavaleri, and P. Lionello, Consiglio Nazionale delle Ricerche, Istituto per lo Studio della Dinamica delle Grandi Masse, Palazzo Papadopoli, 1364 San Polo, 30125 Venice, Italy.

(Received March 18, 1988;
accepted September 16, 1988.)